Materials Advances

ROYAL SOCIETY OF CHEMISTRY

PAPER

View Article Online
View Journal | View Issue

Check for updates

Cite this: *Mater. Adv.*, 2023, 4, 6741

Electrodeposition of PEDOT:ClO_4 on non-noble tungsten microwire for nerve and brain recordings†

Amparo Güemes, ‡[a] Antonio Dominguez-Alfaro,‡[ab] Ryo Mizuta,[a] Santiago Velasco-Bosom,[a] Alejandro Carnicer-Lombarte,[a] Damiano G. Barone,[c] David Mecerreyes[bd] and George Malliaras *[a]

Received 1st November 2023,
Accepted 4th November 2023

DOI: 10.1039/d3ma00949a

rsc.li/materials-advances

Tungsten microwires are commonly used in neuroscience for their high mechanical strength, flexibility, which allows tailoring them to brain and peripheral nerve implantations, and cost-effectiveness compared to other electrode materials. However, challenges such as high impedance and foreign body reactions limit their use as acute and chronic electrophysiology tools. In this work, we propose a novel method for successfully coating tungsten microwires with PEDOT (poly(3,4-ethylenedioxythiophene)) doped with perchlorate anions ClO_4^- using electropolymerization. Pre-treatment of the microwires with annealing resulted in the formation of a WO_3 coating that facilitated the nucleation and deposition of PEDOT, which was more homogeneous than that on gold microwires under the same conditions. *In vitro*, PEDOT decreased the impedance and increased the capacitance compared to bare tungsten microwires. *In vivo*, the PEDOT coating enhanced the signal-to-noise ratio and reduced the standard deviation of noise in acute preliminary electrophysiology recordings of spontaneous activity in the brain and evoked activity in the sciatic nerve of the rat.

Open Access Article. Published on 04 detsember 2023. Downloaded on 01.02.2026 10:58:51.
This article is licensed under a Creative Commons Attribution 3.0 Unported Licence.

1. Introduction

Microwires, also known as microelectrodes, are thin wires typically made of metal that can be utilized to record the electrical signals generated by neurons in the brain.[1,2] Microwires are employed in various research fields including neuroscience, cognitive science, and psychology. They are particularly useful for studying neural activity in the brain as they allow for precise implantation and study of a target anatomical region such as in the hippocampus[3,4] a brain region involved in learning and memory, and in the sensory and motor cortex. Microwires offer additional benefits compared to other neural recording methods. For instance, their small size increases spatial selectivity and reduces tissue damage during implantation, and their high temporal resolution enables the measurement of neural activity with exceptional temporal accuracy.[5,6] Microwires have not only been restricted to interfacing with the brain for recording signals, but they are also capable of recording signals from peripheral nerves.[7–9] The ability to record signals from peripheral nerves using microwires could provide valuable insights into peripheral nerve disorders such as neuropathies, potentially leading to the development of new prosthetic devices. Furthermore, microwire recordings from peripheral nerves can shed light on the mechanisms of nerve repair and regeneration which can help improve therapies for nerve injuries.

Tungsten (W, atomic number 74) is a non-noble metal, commonly used for recording sites on intracortical microelectrode arrays due to its benefits. W-Microwires possess ideal strength, rigidity, and resistance to wear.[10,11] Moreover, they are less expensive than noble metals such as gold, platinum or iridium. However, tungsten is not resistant to corrosion, and previous studies have observed apparent modification of tungsten microwires after four weeks of *in vivo* implantation, causing potential local toxicity due to diffusion of corrosion products into the cortex, impeding its successful long-term recording.[11,12] Moreover, they have relatively high electrical impedance which can significantly affect the quality of the recording signals in the acute and chronic setups. For these

[a] *Electrical Engineering Division, Department of Engineering, University of Cambridge, 9 JJ Thomson Ave, Cambridge, CB3 0FA, UK. E-mail: gm603@cam.ac.uk*
[b] *POLYMAT, University of the Basque Country UPV/EHU, Avenida Tolosa 72, Donostia-San Sebastián, Gipuzkoa 20018, Spain*
[c] *Department of Clinical Neurosciences, University of Cambridge, University Neurology Unit, Cambridge Biomedical Campus, Cambridge CB2 0QQ, UK*
[d] *IKERBASQUE, Basque Foundation for Science, 48009, Bilbao, Spain*

† Electronic supplementary information (ESI) available. See DOI: https://doi.org/10.1039/d3ma00949a

‡ These authors contributed equally to this work.

© 2023 The Author(s). Published by the Royal Society of Chemistry

Open Access Article. Published on 04 detsember 2023. Downloaded on 01.02.2026 10:58:51.
This article is licensed under a Creative Commons Attribution 3.0 Unported Licence.

biocompatibility and high impedance limitations, despite its advantages, the use of pure tungsten in medical implants is currently restricted.[13]

The use of conducting polymers to coat electrodes to enhance their electrical properties and biocompatibility has emerged in the last decades. The most widely used material in the field of bio-interface tissue-to-electronics is PEDOT, particularly when doped with polystyrene sulfonate (PEDOT:PSS).[14] Thanks to its volumetric capacitance[15,16] and high electrical and ionic conductivity,[16] PEDOT:PSS drastically reduces electrical impedance allowing for smaller electrode contact, *i.e.* increasing spatial resolution, and improves signal-to-noise ratio for neurophysiological recordings.[17] Moreover, it is known in the literature that organic coatings can be used to protect metallic substrates from corrosion avoiding the use of heavy metals as corrosion inhibitors. The potential corrosion inhibition capacity of PEDOT has been demonstrated in TiNbZr (TNZ) implants[18] or by forming composites with boron nitride (BN) nanosheets and TiO_2 nanoparticles in 316L stainless steel.[19] Both studies have demonstrated PEDOT as improved barrier protection *in vitro*, improving biocompatibility throughout cell attachment and proliferation.

In this work, we demonstrate the novel coating of W-microwires with PEDOT:ClO_4 conducting polymer. The coating was performed using an electropolymerization (EP) method in an organic solvent, commanded by cyclic voltammetry. We show that treating the W microwires by annealing results in the formation of a WO_3 coating that facilitates the nucleation and homogeneous deposition of PEDOT. The morphology of the deposition was studied and compared with Au/PEDOT. The performance of the novel W/PEDOT microwires for *in vivo* electrophysiology recordings was investigated in two acute exploratory experimental studies: recording low-frequency local field potentials in the brain and high-frequency compound action potentials from the sciatic nerve in the rat model. This approach has the potential to make advanced neuroscience research techniques more accessible to a wider range of researchers and ultimately advance our understanding of the brain and nervous system.

2. Results

Tungsten (W) microwires were originally protected with an insulator layer of Kapton®. Fig. 1A shows the W-microwire when the Kapton® layer was just stripped with a scalpel or annealed afterwards at ~2000 °C in standard conditions (25 °C and 1 atm). For stripped control W-microwires, Raman spectroscopy revealed two main peaks located at ~1350 cm^{-1} and ~1580 cm^{-1}, which could be identified as D and G peaks. These two peaks could correspond to the presence of sp^2-hybridized carbon atoms, present in disordered graphitic materials.[20] They might have been generated by the abrasive action of the scalpel on the polyimide. On the other hand, subsequent removal of any additional residuals of the insulator layer using an annealing process resulted in the formation of a coating of tungsten oxide, which was demonstrated by the

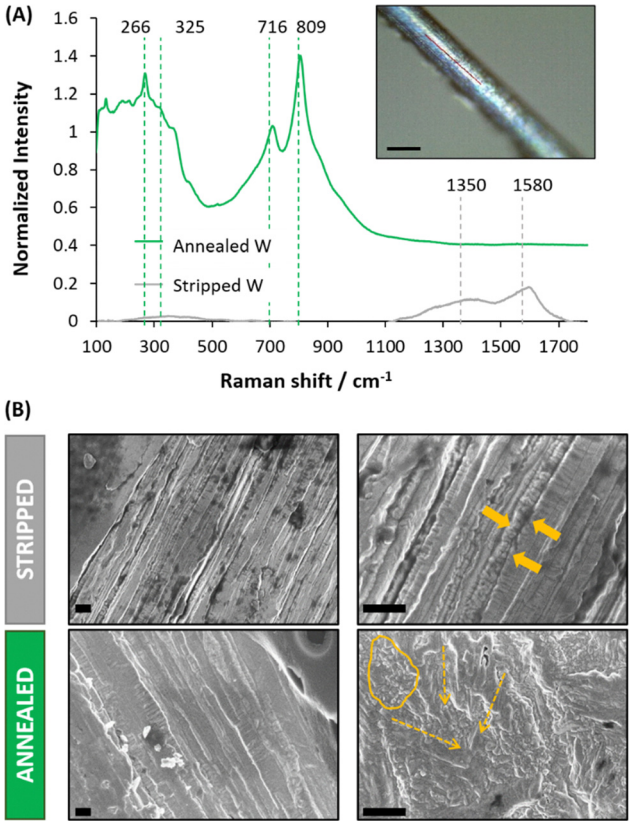

Fig. 1 (A) Raman spectroscopy of annealed and stripped W-microwire. The presence of WO_3 species are labelled at 266, 325, 716 and 809 cm^{-1} while graphitic sp^2-hybridized are present at 1350 and 1580 cm^{-1} (inset: annealed W microwire, scale bar: 70 μm), (B) SEM of W-microwires treated by only stripping (stripped) or stripping plus annealing (annealed) for the removal of the insulator layer of Kapton® (scale bar: 1 μm). The yellow arrows indicate the differences on the microwire morphology.

presence of a first peaks band at 272.2 and 325.5 cm^{-1} induced by W–O–W bending mode vibration and the second band at 718.1 and 807.8 cm^{-1} that corresponds to W–O–W stretching vibration mode.[21] These results confirmed the formation of WO_3 coating on the pristine W-microwire.

Changes in the morphology of the W-microwire can be observed in the Fig. 1B, where the stripped W-microwire presented an aligned and stacked metal surface, while the annealed W-microwire presented the formation of more rough structures, identified as rod-like and amorphous particles morphologies. This mixed morphology suggests the mobility of the deposited metal oxide species over the substrate when annealing, resulting in the formation of WO_3 nanorods. This observation is in agreement with previous reports of W depositions at high temperatures and air-controlled atmospheres.[22,23] Fig. S2 (ESI†) shows the SEM-EDX analysis of stripped and annealed W-microwire. The elemental analysis displayed the presence of oxygen, carbon and tungsten elements. Moreover, if compared to stripped W-microwire, oxygen presence was increased 100 times when the W-microwire was annealed. This observation confirmed that the annealing process followed in this work fully removes the insulator layer resulting in

© 2023 The Author(s). Published by the Royal Society of Chemistry

Open Access Article. Published on 04 detsember 2023. Downloaded on 01.02.2026 10:58:51.
This article is licensed under a Creative Commons Attribution 3.0 Unported Licence.

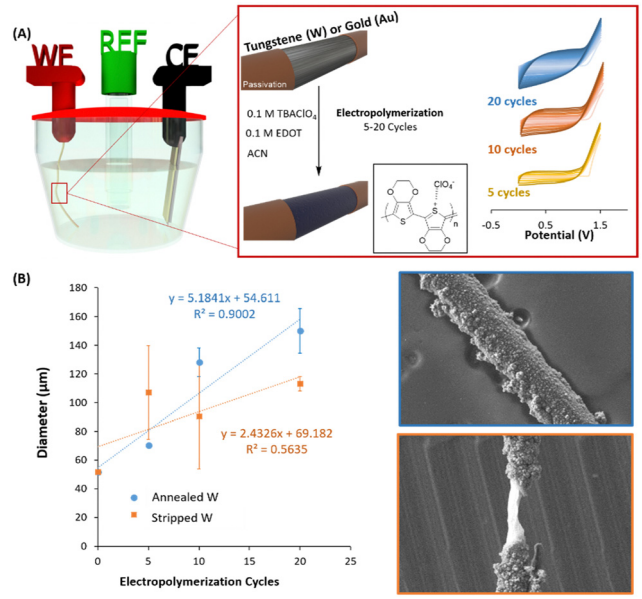

Fig. 2 (A) Schematic representation of the three electrochemical cell where the microwire is used as working electrode (WE), Au/PET as the counter electrode (CE) and Ag/AgCl as the reference electrode. The reaction is performed over the treated area of the microwire, performing the PEDOT coating at 5, 10 or 20 scans around the pristine metal and (B) coating evaluation for one annealed and one stripped W-microwire in cycles-function (n = 5 measurement repetitions each) (left) and SEM images of the heterogeneity of 10 cycles PEDOT deposition on annealed and stripped W-microwire (right).

the formation of WO_3 species coating the surface of the W-microwire.

PEDOT was then electropolymerized in a three electrode electrochemical cell, using the annealed, stripped tungsten (W) or gold (Au) microwires as a working electrode (see Fig. 2A). The electropolymerization was performed and compared within the positive range from 0 V to +1.5 V at three different scan cycles, *i.e.* 5, 10 and 20. Acetonitrile (ACN) and $TBAClO_4$ were used as a solvent and supporting electrolytes, respectively. Fig. 2A shows an increase of the current for each cycle of the deposition, therefore confirming the successful deposition of electroactive material.[24]

The process of electropolymerization of conjugated polymers involves (1) the formation of oligomers in solution, (2) the deposition, which includes nucleation, growth, and (3) the coupling under solid-state conditions.[25] The nature of the nucleation is associated with the metal surface of the electrode and can be evaluated by the so-called nucleation loop, which was first described by Pletcher during the electrodeposition of pyrrole.[26] This phenomenon is normally observed during the very first voltammetric cycle of an electropolymerization experiment. Fig. S3A (ESI†) shows the crossing effect of the PEDOT:ClO_4 deposition that appeared in the first voltammogram of Au/PEDOT. On the contrary, annealed W/PEDOT did not present this loop and was characterised by a straight up/down curve. The behaviour of Au/PEDOT deposition is typically observed when freshly polished electrodes are used for the nucleation process of the conducting polymer.[25,27] As pointed out by Heinze *et al.*,[27] the loop effect is based on a homogeneous reaction from an intermediate oxidized oligothiophene with the starting radical. It is an autocatalytic mechanism, which considerably facilitates the starting oxidation of the monomer. Studies by Zotti *et al.*[28] carried out with redox-active films of conducting polymers indicate similar electrocatalytic effects as observed during voltammetry multi-sweep experiments. Fig. S3B (ESI†) shows clear differences in the deposited morphology when PEDOT is electropolymerized on tungsten and gold microwire, creating nanowires-like morphology in Au/PEDOT while a mixture between nanowires and nanoparticles in W/PEDOT devices.

Once the differences during the nucleation depending on the nature of the surface were confirmed, we observed the

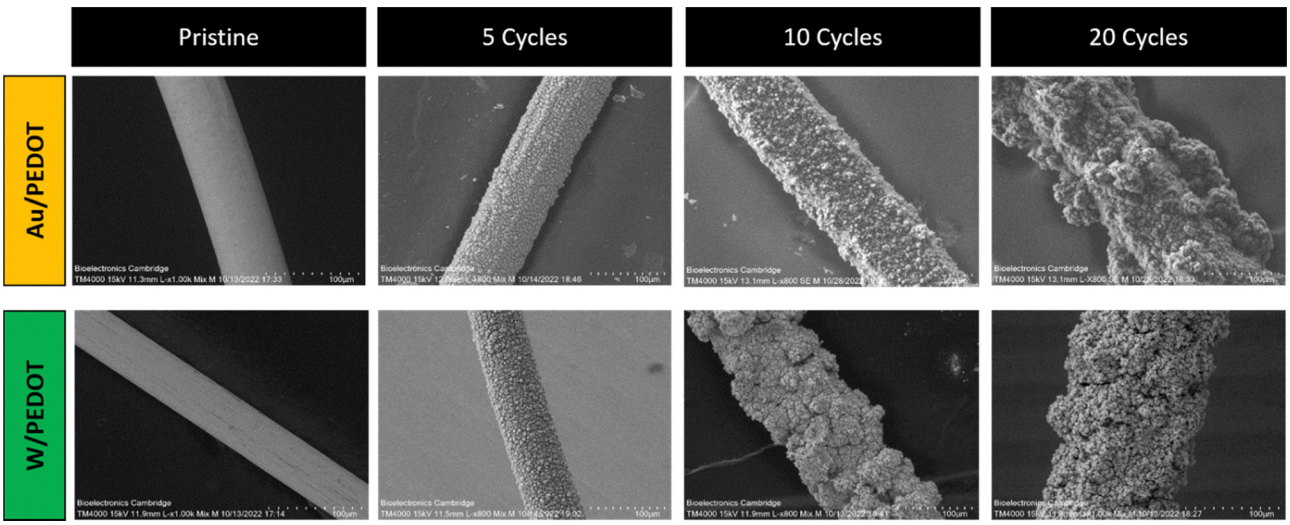

Fig. 3 SEM of pristine Au and W microwires and Au/PEDOT and W/PEDOT electropolymerized at 5, 10 and 20 cycles in 10 mL of ACN, 0.1 M EDOT and 0.1 M of $TBAClO_4$ (scale bar: 100 µm).

Open Access Article. Published on 04 detsember 2023. Downloaded on 01.02.2026 10:58:51.
This article is licensed under a Creative Commons Attribution 3.0 Unported Licence.

differences during the polymerization when the annealed and the stripped W-microwires were used. Fig. 2B shows the diameter of W-microelectrode depending on the number of electropolymerization cycles applied. We found a linear relationship with the polymerised diameter when the W microwire was annealed (R^2 = 0.9002). On the contrary, an important discontinuity was observed when the W-microwire was stripped (R^2 = 0.5635). As confirmed by the SEM images of Fig. 2B, the presence of WO_3 species generated more homogeneous coatings while the bare metal produced imperfections and remarkable heterogeneities. Thus, in this study, we have confirmed that the only way to electropolymerization of PEDOT on W-microwires is through a preliminary treatment that generates oxidized species that assist during the nucleation of PEDOT.

PEDOT electropolymerization achieved in ACN showed homogeneously distributed PEDOT, covering the device surface (see Fig. 3). These results are consistent with previous observations of PEDOT:BF_4 and PEDOT:ClO_4 electropolymerized on stain-steel and Pt/Ir microelectrodes in the same solvents.[29–31] As observed in Fig. 3, PEDOT deposition increased the diameter of the microwire as scans were applied. It is worth pointing out that a smaller number of cycles preserved the morphology of the fibre, generating a smoother surface. When a larger number of cycles were used (10 and 20 cycles), the conducting polymer started to nucleate and grow on the already deposited electroactive material, producing aggregates. This heterogeneous effect was more dramatically observed in the case of Au/PEDOT microwires at 20 cycles, whereas the over-deposition of PEDOT in W-microwire at 20 scans produced micrometre-size porosity and cavities (see Fig. S4, ESI†).

Cyclic voltammetry of W/PEDOT and Au/PEDOT after electropolymerization confirmed the redox activity of the coating. Fig. 4A presents a comparison between W/PEDOT polymerization carried out at different cycles. 5 cycles (5C) of W/PEDOT presented a broad CV than bare metal, confirming the increase in the electroactivity of the material. Moreover, the spectra presented an anodic and cathodic peak above −0.2 V and −0.8 V, respectively. 10 cycles (10C) and 20 cycles (20C) increased the electrical current as a function of the amount of material deposited, with the curves showing a shift in the anodic peak from −0.25 to 0.1 V for 10C and 20C respectively. On the opposite, the cathodic peak remained practically constant at −0.60 V. This behaviour was similar to the observed in Au/PEDOT coating. In this case, the CVs presented a less redox and more pseudo-capacitive behaviour for all the conditions (see Fig. 4D).

In order to characterize the area of the electroactive coating formed, ferrocyanide was used as an outer sphere redox probe as an indicator of electronic coupling between the electrode and the probe (see the reaction scheme in Fig. S5A, ESI†). W microwires in the presence of ferrocyanide present a linear dependence of the anodic or cathodic current with respect to the square root of scan rate, indicating a reversible electron transfer process while for W/PEDOT microwires the anodic and cathodic currents are lineal to the scan rate and correspond to a quasi-reversible process.[32,33] (Fig. S5B–E, ESI†) Interestingly, all PEDOT coating presents a two-electron transfer process (anodic potentials: 0.1 and 0.3 V, cathodic potentials: 0.07 and 0.2 V), being more remarkable as more cycles used for the electrodeposition (20C W/PEDOT > 10C W/PEDOT > 5C W/PEDOT). This dual electron transfer could be attributed to the adsorption of ferrocyanide reactants ($[Fe(CN)_6]^{3-}$) during the ion-exchange process, generated throughout the adsorption anions as co-dopants of ClO_4^-. As a consequence, there is observed a non-reversible anodic peak in 10 W/PEDOT microwires at low

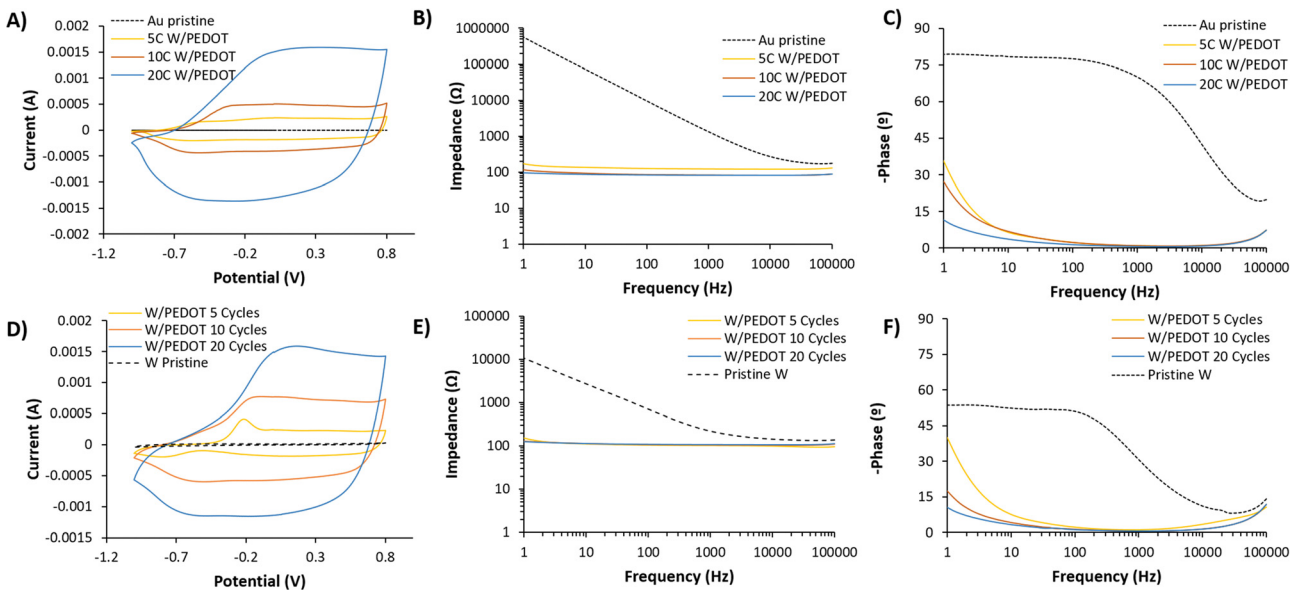

Fig. 4 (A) Cyclic voltammetry, impedance (B) and (C) phase measured of bare tungsten (W) and 5, 10 and 20 cycles coated W/PEDOT in 0.1× PBS as supporting electrolyte in water, (D) cyclic voltammetry, impedance (E) and (F) phase measured of bare gold (Au) and 5, 10 and 20 cycles coated Au/PEDOT in same conditions.

© 2023 The Author(s). Published by the Royal Society of Chemistry

Open Access Article. Published on 04 detsember 2023. Downloaded on 01.02.2026 10:58:51.
This article is licensed under a Creative Commons Attribution 3.0 Unported Licence.

scan rates (25–100 mV s^{-1}) (Fig. S5D, ESI†) and more clearly observed in 20 W/PEDOT microwires at a range from −0.52 to −0.23 V (Fig. S5E, ESI†).[34]

By using the Randles–Sevcik equation, the electroactive surface area of W and W/PEDOT microwires was estimated.[35] The modification W-microwire with PEDOT enhances up to two orders of magnitude the electroactive area (see Fig. S6, ESI†). Indeed, W microwires present an electroactive area of 1.4×10^{-6} cm^2 and W/PEDOT microwires present 4.36×10^{-5}, 2.98×10^{-4} and 7.19×10^{-5} for 5C, 10C and 20C respectively. This result points out the superior electrochemical micro-platform of W/PEDOT if compared to bare W microwires.

The coating of PEDOT on the electrode plays an important role in the reduction of the electrode impedance. When bare metals were evaluated (W or Au), the capacitance remained dominant even at very low frequencies, confirmed by the slope of the impedance below 1 kHz (Fig. 4B and E) and the value of – phase (°) at 1 Hz, *i.e.* −53 and −80° for W and Au respectively. The data fitted a simple Randle's circuit, where the impedance at the interface of the electrode and the solution is produced by a double-layer capacitance in parallel with a resistance of the charge transfer of the bare metal electrode (see Fig. S7, ESI†). Conversely, for the conductive polymer-coated electrodes, the resulting impedance is dominated by a resistive and capacitance contribution in high and medium-low frequencies respectively. This equivalent circuit was proposed by Bianchi *et al.*[36] to describe the electrochemical impedance interface for PEDOT:PSS coated microelectrodes during *in vitro* measurements. This contribution at medium-low frequencies is observed by the slight increase of the interface impedance related to the double layer capacitance at lower frequencies (1 Hz), observed as a result of the increase of – phase (°) from −10° for 20C W/PEDOT to −35° for 5C W/PEDOT (see Fig. 4B, C, E and F). The values of impedance fitted were above one order of magnitude higher for pristine metals (1 530 000 Ω for Au and 6770 Ω for W) compared to Au/PEDOT (126, 86.7, 83.4 Ω for 5, 10 and 20 cycles) and W/PEDOT (160 ± 20, 210 ± 107, 83.4 Ω for 5, 10 and 20 cycles). Similarly, the capacitance values extracted from the fitting circuits ranged from 0.000 189 (pristine Au) to 6.85 mF (20 cycles Au/PEDOT) and 0.000 032 ± 0.000 014 (pristine W) to 2.48 ± 0.102 mF (20 cycles W/PEDOT). These results for resistivity, capacitance, as well as the goodness of the fitting to the circuits shown in Fig. S7 (ESI†) are summarized in Table S1 (ESI†).

2.1 Feasibility of the tungsten microwires coated with PEDOT for brain recordings

A preliminary investigation was conducted to evaluate the performance of the tungsten microwires coated with different amounts of PEDOT (5C and 20C) compared to the use of traditional uncoated tungsten microwires devices comprising two shanks for paired comparisons were assembled and implanted *in vivo* to record spontaneous activity from the barrel cortex in the rat. We designed the shanks of the probe to be around 300 μm apart. Approximately 3 mm were exposed at the tip of the microwires (2.7 ± 0.1 mm, Fig. S1, ESI†), which limited the ability of the microwires to detect single-unit activity. Therefore, in the first experimental scenario, the devices were implanted in the sensory cortex of the brain for assessing their ability to record local field potentials (see Fig. 5A). Two consecutive implantations of the two different electrodes were conducted in the same animal. Details of the implantation can be found in the Experimental section. The barrel cortex is formed by the arrangement of clusters of neurons called barrels. These barrels are specialized to receive input from a specific whisker and are arranged in a topographic map that corresponds to the position of the whiskers on the animal's face. Its large size within the somatosensory cortex and the large number of neurons arranged in it made it a good location to evaluate the devices in the brain. The recording of local field activity comprised alternating periods of spontaneous rest and activity as illustrated in the low-frequency recording traces obtained with the 5C W/PEDOT and W microwires shown in Fig. 5B. Each pair of rest and activity periods with a duration of at least 2 seconds each was considered an observation (see zoom inserts in Fig. 5B). A total of 20 observations were obtained using the device assembled with the 5C W/PEDOT microwire coated and the uncoated microwire, and a total of 11 observations were obtained using a device comprising a coated 20C W/PEDOT microwire with an uncoated microwire. The signal-to-noise ratio (SNR) and the standard deviation of the resting period (STDr – measure of the background noise) was computed for each observation, and paired statistical tests were applied over all observations for comparing each pair of microwires within each device (representative example of the 20C W/PEDOT *vs.* W comparison shown in Fig. 5C). The Shapiro–Wilk tests applied over each independent group (*e.g.* SNR of all observations using the uncoated microwire) failed to reject the null hypothesis in all groups, and therefore the normality criteria were met in both comparisons. Parametric paired *t*-tests could also be applied to both SNR and STDr statistical analysis to compare the microwires within the first device (5C W/PEDOT *versus* uncoated wire) and second device (20C W/PEDOT *versus* uncoated wire) after confirming equal variances using the Levene's test. The differences in the mean SNR were significant between the 5C W/PEDOT and bare microwires (SNR: 9.99 ± 2.97 dB in 5C, 9.27 ± 2.46 dB uncoated with $p = 0.046$), but were not significantly different when comparing the STDr between the two microwires (18.56 ± 4.66 5C *vs.* 19.19 ± 6.34 uncoated, $p = 0.34$). When comparing the microwire coated with 20C W/PEDOT and the uncoated microwire using the paired *t*-test, differences in results were very significant for SNR (7.25 ± 1.38 dB in 20C, 2 ± 1.84 dB in uncoated with $p = 0.0008$), and STDr (31.09 ± 5.67 μV in 20C, 100.27 ± 34.13 μV uncoated with $p = 0.004$). Importantly, the two pairs of comparisons (5C W/PEDOT *vs.* W and 20C W/PEDOT *vs.* W) cannot be compared between them because each of them underwent a different implantation. SEM images of the 20C coated electrodes post-implantation showed a decrease of 22.6% of the diameter of the PEDOT deposition after implantation (150 μm pre-implantation to 116 μm post-implantation) (Fig. 5D), which did not affect their recording performance. In fact, the fold change in impedance of the 20C coated electrodes over the bare ones at

Open Access Article. Published on 04 detsember 2023. Downloaded on 01.02.2026 10:58:51.
This article is licensed under a Creative Commons Attribution 3.0 Unported Licence.

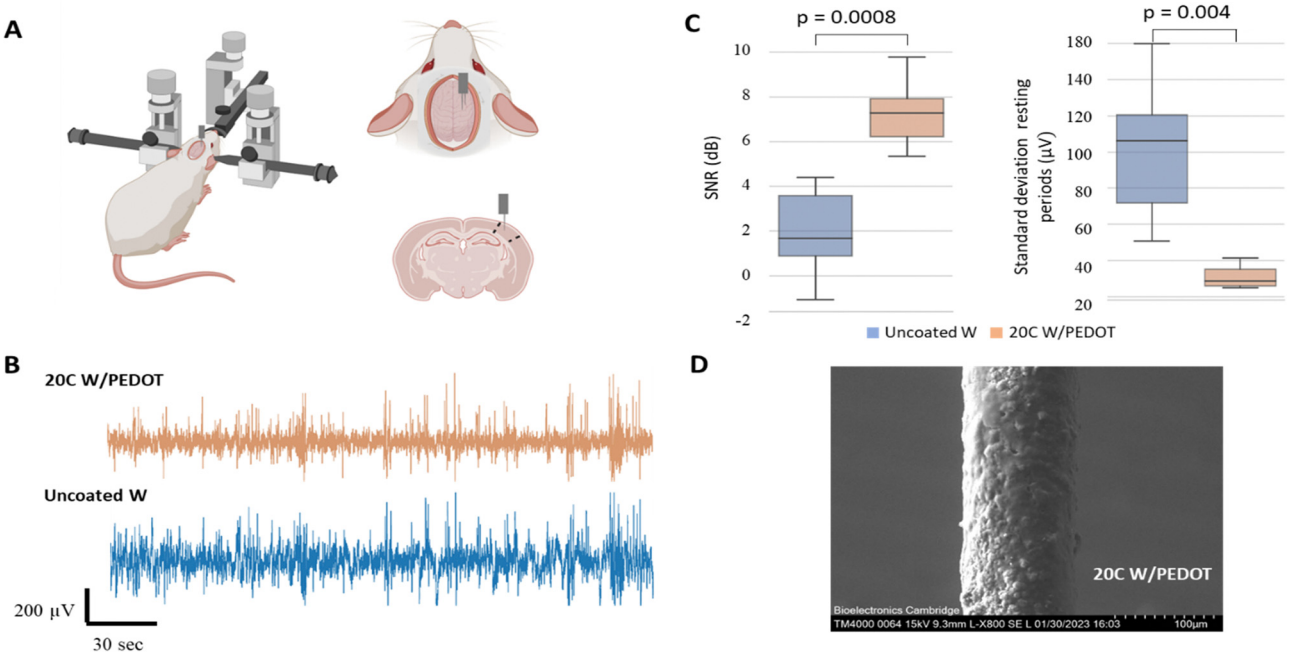

Fig. 5 Illustration of the two-shank 20C W/PEDOT – W microwire probes for recording spontaneous activity in the brain. (A) Cartoon showing the surgical setup (left) and the implantation of the probe with the shanks oriented along the AP axis (right-top) in the Barrel cortex depicted in the coronal section map (right-bottom). Created with biorender.com. (B) Illustrative low-pass filtered recording (<200 Hz) traces from the 20C W/PEDOT microwire (top) and the bare W microwire (bottom) showing local field spontaneous activity with alternating periods of rest and activity. (C) Box plots showing the comparison of SNR and standard deviation of the signal in the resting periods for the device pair (20C W/PEDOT *vs.* uncoated W). Negative SNR means that in some instances the signal power was lower than the noise power. (D) SEM of the 20C W/PEDOT microwire post-implantation (scale bar: 100 µm).

1 kHz when implanted *in vivo* was 2.83, which aligns with the fold change in SNR of 3.62, the fold change of STDr of 3.22, and with the values obtained pre-implantation *in vitro* at 1 kHz (approx. 2.5).

2.2 Feasibility of the tungsten microwires coated with PEDOT to record in peripheral nerves

Once the ability of the microwires to record low-frequency signals like local field potentials (LFPs) in the brain was evaluated, a second exploratory study to analyse their potential to record improved high-frequency evoked compound action potentials (CAPs) from peripheral nerves was assessed. Similar to the previous experimental setup, devices comprising two shanks for paired comparison of microwires with different amounts of PEDOT coating (no coating, 5C and 20C) were assembled and implanted around the sciatic nerve of the rat for recording fast compound action potential. Consecutive implantations of devices with different amounts of coating were conducted in the same animal. Details on the experimental setup can be found in the Experimental procedures section and are illustrated in Fig. 6A.

To examine the impact of PEDOT coating on the quality of the recordings, the standard deviation of the baseline period of band-pass filtered recordings (200–7000 Hz) prior to the stimulation was compared (Fig. 6B). We found that the coating significantly decreased the mean standard deviation of the baseline period compared to the recordings obtained with the uncoated tungsten microwires (device 1 (p = 0.0002): 3.14 ± 0.22 µV) from the uncoated microwire, 2.84 ± 0.14 µV from microwire coated with 5C of PEDOT; device 2 (p = 0.03 : 2.94 ± 0.43 µV from the uncoated microwire, 2.7 ± 0.24 µV from microwire coated with 20C of PEDOT). We also found that the values of the impedances of the coated microwires were similar among them and approximately halved compared to those of the uncoated microwires (fold change of 2 and 1.85 for the 5C and 20C with respect to bare microwires, respectively). The similarities in impedance order independently of the amount of coating once again suggests that other sources of impedance are more predominant in the recording circuit and the reduction provided by the wires becomes less significant.

The ability of each microwire to discriminate the activation of different fibre types was also evaluated from extracted CAPs profiles elicited by different stimulation protocols. In general, any peripheral nerve that consists of different fibre types with varying velocities can produce a CAP waveform when stimulated. The CAP waveform is considered the activation profile of the nerve as it represents the sum of the individual single-fibre action potentials. In fact, each peak in the CAP profile is an indication of a fibre population being activated with a specific velocity. When the recording and stimulation electrodes are positioned at a specific distance, it results in a high-resolution recording because the CAP components with different fibre velocities are separated temporally, as illustrated in different shadow-coloured regions in Fig. 6C and D. As the stimulation current increases, a greater number of fibres are activated, resulting in an increasing number of peaks on the CAP waveform as shown in the Fig. 6D.

© 2023 The Author(s). Published by the Royal Society of Chemistry

Open Access Article. Published on 04 detsember 2023. Downloaded on 01.02.2026 10:58:51.
This article is licensed under a Creative Commons Attribution 3.0 Unported Licence.

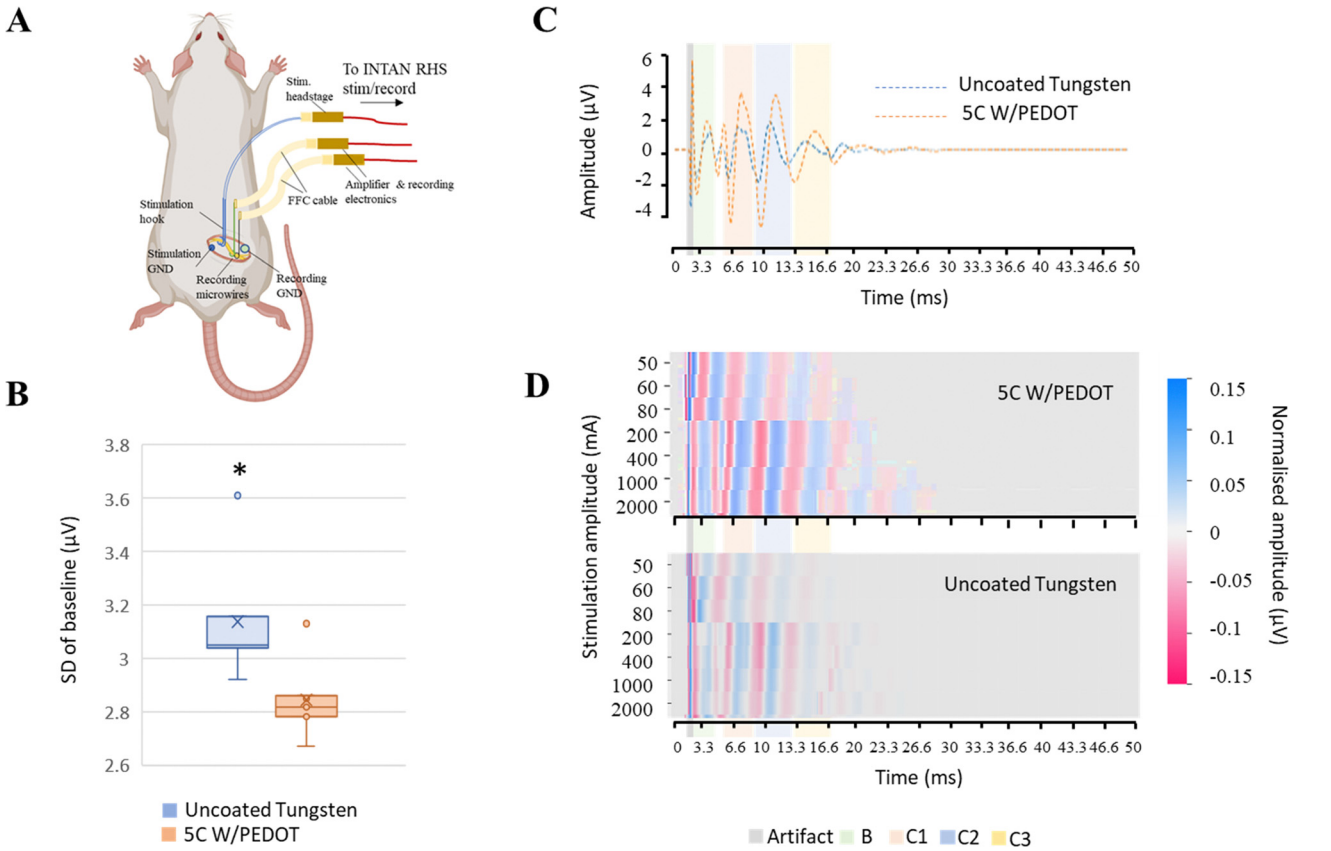

Fig. 6 Illustration of the two-shank 5C W/PEDOT – W microwire probe for recording of evoked CAPs in the sciatic nerve. (A) Cartoon showing the electrophysiology setup with a stimulation bipolar hook probe implanted rostrally and W microwires implanted in pairs caudally (created with biorender.com). (B) Boxplot showing the comparison of the standard deviation of baseline for the first device pair (5C W/PEDOT) *vs.* uncoated W, * p = 0.0002. PEDOT coating reduced the impedance and the noise background compared to the bare wires. (C) Average evoked CAPs (20 repetitions, using singles pulses at 400 mA and 0.1 ms) extracted from each microwire using a window of 2 ms before and 10 ms after the stimulation artefact (grey region). Interestingly, a slight delay due in the CAP peaks can be noticed due to the separation between the two wires in the nerve (approximately 2 mm), becoming more noticeable at the slower C-fibre peaks. Coloured regions correspond to the resolution of different fibre populations based on conduction velocities. (D) A representative colour-map representation of the CAP activation elicited by each stimulation amplitude at 0.1 ms pulse width where C3 and C4 fibre peaks can be resolved at longer times (up to 27 ms of the evoked CAP) using the coated microwire (top: 5C W/PEDOT, bottom: uncoated W).

Average CAPs for each stimulation protocol and microwire from a minimum of 10 stimulation pulses were extracted using a window of 2 ms before and 50 ms after the stimulation artefact (Fig. 6C). The activity of each fibre type could be distinguished by looking at the timing of the activity relative to the distance between the stimulation and recording sites (L = 1 cm ± 0.05 cm) and calculating the conduction velocity. A representative colour-map representation of the CAP activation elicited by each stimulation protocol is shown in Fig. 6D, where new peaks can be resolved with larger stimulation intensities. Coating the microwires with PEDOT allowed us to visualise peaks at longer times, *i.e.* to resolve the activity of slower C3 and C4 fibres at a lower stimulation strength. This difference was more notable when comparing single traces of the average CAP profiles (see Fig. 6C), where larger amplitudes were recorded using the coated microwires.

3. Discussion

In this study, we have demonstrated a novel strategy to deposit poly(3,4-ethylenedioxythiophene) (PEDOT) on tungsten (W)-microwires consisting of electropolymerization. This study has established that the preconditioning of W-microwires through annealing to generate oxidized species in the surface is necessary for the successful electropolymerization of PEDOT doped with perchlorate anions ClO_4^- (PEDOT:ClO_4) by facilitating its nucleation. The improved electrochemical properties of the resulting W/PEDOT microwires were further demonstrated in acute *in vivo* experiments for brain and peripheral nerve recordings, which illustrate two important fields of application for progress in electrophysiology studies.

Tungsten microwires are a commonly used type of microelectrode for recording neural activity due to their high mechanical strength and resistance to breaking.[10,11] However, several limitations restrict their use. One major limitation of tungsten microwires is that they have a relatively high impedance. Impedance is a measure of the resistance of an electrode to the flow of electrical current. High impedance can cause a reduction in the amplitude of the recorded signals, which can make it more difficult to detect and analyse neural activity. Coating electrodes with PEDOT has been demonstrated to be a

Open Access Article. Published on 04 detsember 2023. Downloaded on 01.02.2026 10:58:51.
This article is licensed under a Creative Commons Attribution 3.0 Unported Licence.

successful strategy for reducing impedance in electrophysiology recordings compared to bare materials by significantly improving electrical conductivity.[37–39] Our approach has the potential to make advanced neuroscience research techniques more accessible to a wider range of researchers and ultimately advance our understanding of the nervous system.

The deposition of PEDOT in complex and conductive geometries such as microwires has traditionally been most commonly accomplished using electropolymerization.[31,40–42] This method enables precise control over the amount of material deposited, dopant concentration, and monomer functionality. Although it presents difficulties in terms of scalability as a coating methodology, its application is still viable for microwires. The morphology, biocompatibility, electrochemical properties, and stability of the resulting device can be influenced by carefully adjusting the doping process. Authors have shown that the use of the solvent could change the process of nucleation, besides impact the morphology of the deposition. For example, it was demonstrated that organic solvents such as polycarbonate and acetonitrile (ACN) produce fibrillary structures, whereas deionized water produces roundish particles decorating the surface of the electrode. Moreover, organic solvents produce more stable and adhesive coatings. If dopants are used, they can be tuned to improve functionality. For example, PEDOT:ClO_4 and PEDOT:BF_4, reported high charge storage capacity. Vara *et al.* doped PEDOT with poly(4-styrenesulfonic acid-*co*-maleic acid) (PSS-*co*-MA) on carbon microwires for the bio-conjugation of macromolecules.[43,44] Doping of PEDOT:PSS with polydopamine created an adhesive thin layer that formed a stable interpenetrating network for long-term stability as a neural interface.[45] PEDOT doped with carboxyl functionalized multi-walled carbon nanotubes (CNTs) demonstrated to outperform the traditional PEDOT/PSS, showing improvement in terms of chronic electrode stability and impedance over 4 months when implanted in the visual cortex.[39] Other more innovative methodologies as support-free PEDOT:PSS microwires manufactured by wet-spun have been also reported for recording and for modulating neural activity.[46,47]

In this study, we conducted an exploratory study on the ability of the developed W/PEDOT microwire devices to record spontaneous low-frequency information from large brain regions by implanting it into the barrel cortex of rodents. The barrel cortex in rodents is composed of numerous small units that process sensory information from individual whiskers, making it an ideal model for neuroscience research. Its unique structure has made it a popular subject of study. The large area exposed at the tip of each microwire for visualisation and comparison purposes allowed us to record local field potentials (LFPs) from the Barrel cortex. Alternatively, work for single-neuron recordings can be similarly achieved by cutting the microwires and coating only the exposed part at the tip. LFPs are the extracellular potentials that are generated by the collective activity of many neurons in a specific area of the brain. Due to their high temporal resolution, they can provide information about the synchrony and timing of neural activity, as illustrated by the patterns of rest and activity observed in our recordings. LFP signals are typically low-amplitude and require a high-quality amplifier to be accurate. In this exploratory study, coating the microwires significantly improved the SNR of the recorded signals, with a thicker coating having a more substantial effect on improving the signal quality. These results align with a previous study that records from the thalamus using PtIr.[41] In that study, PEDOT coating reduced the impedance and led to a better signal-to-noise ratio compared to the bare electrode. Similar outcomes were obtained when recording EMG signals from the neck using PEDOT/stainless steel wires.[42]

In addition to the brain, the study of electrophysiology in peripheral nerves is increasingly gaining attention in the last decades, especially since the attraction of targeting peripheral nerves to diagnose and treat disorders using bioelectronic medicine. In recent years, advances in technology have enabled the development of new tools for peripheral nerve electrophysiology, which allow for the recording of signals from many nerve fibres simultaneously. These advances have increased the accuracy and resolution of electrophysiology recordings, leading to new insights into the functioning of the peripheral nervous system. In this work, we contribute to this progress by presenting the potential use of tungsten microwires coated with PEDOT to study high-frequency fibre evoked activation within the sciatic nerve of the rat. In general, the quality of the recorded signal can limit our ability to resolve smaller peaks, which generally relate to smaller and slower fibres that are recruited last (C fibres). Therefore, strategies to improve the SNR of the recorded signals, either by increasing the amplitude of the signal of interest, or reducing the amplitude of the background noise, or a combination of both, are needed to increase our understanding of the propagation of action potentials by different fibre types. Coating the tungsten microwires with PEDOT resulted in reduced background noise compared to uncoated wires. The origin of this drop in the standard deviation of the baseline signal may be related to a drop in the impedance of the coated devices to half of the value of the uncoated ones or the increase in the electrochemical area by one order of magnitude. These improved preliminary outcomes are of great importance in peripheral nerve recordings as tungsten microwires have recently been proposed as a successful strategy to record intraneural recordings from the cervical vagus nerve in awake humans.[48]

It is worth mentioning that PEDOT coating promotes the reduction of the faradaic reactions of W-microwires, which refers to the electrode's ability to participate in redox reactions with the surrounding electrolyte. As described by Malliaras *et al.*, a capacitive response is desirable in neural electrodes instead to avoid the generation of reactive species, such as H_2O_2.[49] This is very relevant in electrical stimulation electrodes, but also in photovoltaic-based stimulation electrodes, where the capacitive mechanism relies on disturbing the ions at the electrolyte/electrode interface that results in the generation of stimulating potential fields on the cell membrane.[50] Therefore, pseudo-capacitance or capacitance properties of the material offer a rapid and safe charge-injection approach for neural

© 2023 The Author(s). Published by the Royal Society of Chemistry

Open Access Article. Published on 04 detsember 2023. Downloaded on 01.02.2026 10:58:51.
This article is licensed under a Creative Commons Attribution 3.0 Unported Licence.

stimulation by effectively suppressing redox reactions and minimizing heating effects. However, this charge injection needs to be sufficient to induce neural activity without exceeding potentials for irreversible electrochemical reactions and producing cytotoxic species[50,51]

The effects of reducing electrode impedance on improving signal-to-noise ratio (SNR) and signal quality in *in vivo* neural recordings are still a subject of debate. Some studies have shown that low-impedance electrode coatings can enhance SNR both in acute and chronic setups by reducing thermal noise[52] and low-frequency artifacts,[53] and increasing the signal for local field potential and for spikes,[52–55] which aligns with our observations in this study. However, other research has suggested that high-SNR recordings can be achieved with microelectrodes exhibiting a range of impedances, implying that extremely low impedances may not be necessary for optimal SNR.[56,57] To the best of our knowledge, there is still no published evidence indicating that lower-impedance microelectrodes lead to lower recording quality, but further investigation and full characterisation of the electrodes are required to fully understand the impact of coating on the quality of the recorded signals in acute and long-term *in vivo* recordings.

Future research is needed to fully characterise the performance of our W/PEDOT microwires *in vivo* in a larger experimental sample size to provide a thorough validation of the presented preliminary results. In addition, the capability of this new material to record over chronic conditions should be evaluated, but coating with PEDOT appears to be a definite solution to increase the use of tungsten microwires in electrophysiology. Bare tungsten microwires can be affected by electrochemical reactions, which can cause a build-up of resistance over time and can lead to drift in the recorded signals, making it difficult to obtain accurate long-term recordings. However, coating the microwires with PEDOT has been reported to help to reduce the inflammatory process and the formation of scar tissue and granulomas around the microwire, which can improve the long-term stability and performance of the device.[41,42] Furthermore, PEDOT coating also could potentially provide a protective barrier for the tungsten microwires that helps to reduce the number of tungsten ions that are released into the surrounding tissue, improving the safety and biocompatibility of the device. Finally, conducting polymers have been demonstrated to protect metallic substrates from corrosion and, in some cases, inhibit the oxygen reduction at the delamination front of the conducting coating, forming a ''protection zone'' that reduce remarkably the corrosion-driven coating delamination. This was demonstrated with polyaniline, polypyrrole and PEDOT:PSS.[58,59] However, previous studies have demonstrated that PEDOT's delamination can depend on various factors such as the substrate it is deposited on, the dopants and concentrations used,[60,61] the intended use of the electrode for recording or stimulating applications (D_{ijk}), and the duration of exposure. Also, there is a possibility for PEDOT to experience cracking and delamination under electrochemical stress or during handling.[54,62–64] Moreover, while PEDOT-coated electrodes exhibit a decreased adverse body response compared to bare metal, it is important to note that the body response can still influence the long-term performance and stability of PEDOT coatings in chronic experiments. Therefore, despite promising, follow-up studies in long-term implantations are needed to validate and characterise the properties and performance of the presented W-microwires coated with PEDOT.

4. Experimental and methods

4.1 Materials

3,4-Ethylenedioxythiophene (EDOT; >97%) was purchased from Sigma-Aldrich; tetrabutylammonium perchlorate (TBA-ClO_4; >99.0%) was purchased from Sigma-Aldrich. Acetonitrile (ACN) was acquired from Sigma Aldrich. All reagents and solvents were used as received with no further purification. Gold (Au) insulated wires (75 μm diameter, PTFE insulation, Goodfellow Cambridge Ltd) and tungsten (W) insulated wires (75 μm diameter, polyamide insulation, California Fine Wire Co.).

4.2 Methods

Removing insulation of microwires. The first step in the functionalization of the microwires was removing the insulation layer at both ends, PTFE for gold (Au) microwires and kapton for tungsten (W) microwires. The insulation removal was carefully performed using rulers and Kapton© tape to ensure accurate control over the total exposed length of the microwire tips (see Fig. S1, ESI†). For Au-microwires, the insulator was gently stripped mechanically with a scalpel. For the W-microwire, the Kapton© was firstly stripped mechanically with a scalpel and then the residuals were burned with a flame during 2 seconds ($T♀ \sim 2000$ °C) at standard conditions *i.e.* 21% oxygen, resulting in the annealing of the wire. A non-burned W-microwire – only stripped – was used as control. The chemical reaction for the burning step could be estimated as follow:[65]

$$2W\ (solid) + 3O_2\ (gas) \rightarrow 2WO_3\ (thin\ film\ coating)$$

PEDOT electrodeposition on metal microwires. PEDOT was electrochemically deposited on the exposed gold (Au) or tungsten (W) microwire areas (area of deposition of $\sim$2.35 mm^2). The deposition was performed in a three-electrode chamber where the metal microwire was the working electrode (WE), Au deposited on PET ($\sim$1 cm^2) served as the counter electrode (CE) and Ag/AgCl as the reference electrode. The deposition was performed using cyclic voltammetries at 50 mV s^{-1} scan rate from 0.0 to +1.5 V. For the reaction, 0.1 M of EDOT as monomer and 0.1 M of TBAClO_4 as supported electrolyte was used in a 10 mL ACN reaction solution three cycles were investigated, *i.e.* 5, 10 and 20. After each deposition process, the resulting microwire was rinsed with ACN and water to remove the unreacted precursors and the electrolyte.

Cyclic voltammetry (CV). CV was used to compare the film formed of 5, 10 and 20 cycles of W/PEDOT and Au/PEDOT, using 50 mV s^{-1} scan rate and −1.0 to +1.0 V in 10 mL of water

Open Access Article. Published on 04 detsember 2023. Downloaded on 01.02.2026 10:58:51.
This article is licensed under a Creative Commons Attribution 3.0 Unported Licence.

with 1× PBS as supported electrolyte. A film of Au/PET was used as counter electrode and Ag/AgCl was used as a reference.

A second set of CV measurements was conducted to characterize the area of the electroactive coating formed. The experiments were performed on W microwire and 5, 10 and 20 W/PEDOT microwires in 1 mM $K_3Fe(CN)_6$ as a probe redox system at different scan rates according to the Randles–Sevcik equation;[66]

$$I_p = 2.69 \times 10^5\, ACn^{3/2}D^{1/2}v^{1/2}I$$

where I_p is the peak current (A), A is the electroactive area (cm^2), C is the molar concentration of $K_3Fe(CN)_6$ solution, n is the number of transferred electron in the redox reaction, D is the diffusion coefficient of redox probe ($cm^2\ s^{-1}$) and v is the scan rate ($V\ s^{-1}$). The $[Fe(CN)_6]^{3-/4-}$ redox system is extensively used to estimate the electroactive surface area of bare/modified electrode in electrochemical characterization. The number of transferred electron (n) is 1 and diffusion constant (D) is 7.6×10^{-6} $cm^2\ s^{-1}$ for 1.0 mM probe molecule in 1 M KCl electrolyte.[35,67]

Electrochemical impedance spectroscopy (EIS). EIS was used impedance of the coated material. Au/PEDOT or W/PEDOT microwire was placed within a three-electrode cell where the microwire was placed as WE, Au/PET as the CE and Ag/AgCl as reference electrode using 0.1 M (pH 7.4) PBS as supported electrolyte and solvent. The measurement was recorded controlling the fibre area, *i.e.*, 2.35 mm^2. Impedance evaluated frequency changes in the range from 0.1 to 100 kHz, with an amplitude of 10 mV, within a Metrohm AG, NL.

Raman spectroscopy. Raman spectra of W and control-W microwires were acquired using a Renishaw InVia Confocal Raman microscope with a laser of 532 nm wavelength with 1 s of integration time and 100% of the power. The selected Raman shift ranged from 100 to 1700 cm^{-1}. The acquisition was performed in mapping mode and each averaged Raman spectrum corresponded to a line shape with the accumulation of at least 180 different points. In the case of W/PEDOT or Au/PEDOT microwires, the measurements were acquired with 532 nm laser wavelength, 1 s of integration time and 1% of power, in order to avoid sample degradation. Control experiment with 10% of power and 1 s was also performed, obtaining similar sp^2 signals at $\sim$1350 cm^{-1} and $\sim$1580 cm^{-1}.

Scanning electron microscopy (SEM-EDX). SEM images were taken on a ZEISS Gemini 300 VP scanning electron microscope using an acceleration voltage of 1 kV and an in-lens secondary electron detector. SEM-EDX mapping was performed with an acceleration voltage of 15 kV at a working distance of $\sim$5 mm, using an Oxford Instruments EDS detector. The microwire was placed on top of carbon tape and analysed in point-by-point scanning mode.

Animal implantation. All animal procedures were carried out in accordance with the UK Animals (Scientific Procedures) Act, 1986. Work was approved by the Animal Welfare and Ethical Review Body of the University of Cambridge and by the UK Home Office (project licence number PFF2068BC). Sprague–Dawley rats (Charles River, UK) were used in this study and were generally received at least 1 week prior to surgery for acclimation. Surgical procedures were done under isoflurane anaesthesia (2.5% in O_2, lowered to 1.25% prior to and during electrophysiology experiments). The animal's body temperature was monitored and maintained throughout the experiments using a thermal blanket. For brain implantation, brain maps were used to locate the middle area of the barrel cortex where the microwires were inserted following a technique published elsewhere.[68] The barrel cortex is located in the primary somatosensory cortex, which is located in the postcentral gyrus of the parietal lobes. After shaving it, the head of the animal was fixed on a stereotaxic frame. The skin and underlying soft tissues were retracted from over the calvarium to expose the skull surface. Next, a 3 × 3 mm^2 cranial window slightly larger than the barrel field region was made on the right hemisphere with a drill (4 to 6 mm lateral to the midline and from 1 to 4 mm posterior to bregma), and then the dura was removed. The probe was mounted onto the frame and lowered into the middle of the region (bregma coordinates −1 to −4 mm AP, 5 mm ML) and inserted always at the same depth of 1.2 mm to ensure the same length of the tip was exposed to the neural tissue for consistency in the recordings. The two-shank devices were aligned along the sagittal plane. Additionally, a stainless-steel screw was drilled into the cerebrospinal fluid above the cerebellum to act as a recording ground. Recordings of spontaneous activity were obtained for 15 minutes. Two consecutive implantations of two different devices were conducted in one animal.

For sciatic nerve experiments, the animal was placed in a prone position. The right gluteal area and lower limb of the rat were shaved and cleaned with an alcohol–iodine solution. A surgical incision, approximately 2 cm in length, was made along the axis of the femur, starting at the gluteus muscle and extending to the mid-thigh. The right sciatic nerve was then exposed from its location in the pelvic cavity to its branching point into the nerve fibularis and nerve tibialis. The nerve was carefully exposed by removing the overlying fascia while preserving the epineural covering. A bipolar stimulation hook was implanted proximal for nerve activation, and the tips of the two-shank devices, which were coated with different amounts of PEDOT (20 cycles, 5 cycles or no coating), were implanted distally around the full circumference of the nerve for the recording of evoked potentials, which ensured that the amount of exposed area of the tip in contact with the nerve was always the same. A 1 cm^2 patch of gold film coated by PEDOT which served as the ground was placed subcutaneously close to the recording site. Consecutive implantations of devices with different amounts of coating were conducted in the same animal.

Electrophysiology and data analysis. All the devices were connected to a 32-channel recording headstage (Intan Technologies, Los Angeles, CA, USA) *via* a custom-built omnetics/ZIF connector PCB and flexible flat cable, and signals were acquired at 30 kHz through the RHS 2000 stimulation/recording controller (Intan Technologies, Los Angeles, CA, USA). The raw data were exported and processed offline with self-written Python

© 2023 The Author(s). Published by the Royal Society of Chemistry

Open Access Article. Published on 04 detsember 2023. Downloaded on 01.02.2026 10:58:51.
This article is licensed under a Creative Commons Attribution 3.0 Unported Licence.

scripts. In all cases, the local references were connected to the ground of the recording hardware.

For sciatic nerve experiments, a single grounding point was used to connect stimulation and recording grounds, which consisted of a film of 1 cm × 1 cm gold film coated by PEDOT placed subcutaneously closed to the recording site. A minimum of 10 single bipolar pulses were applied through the stimulation device for each stimulation protocol, and the evoked activity was recorded by the recording device composed of two microwires with different amounts of PEDOT coating. Two pulse widths (PW) were used for the stimulation protocols (PW = 100 μs and 500 μs). Pulse widths were kept low to limit the duration of the stimulation artefact. For each pulse width, stimulation current (I) was varied through different values: for pulse width 0.1 ms the stimulation current ranged from 50 μA up to 2 mA (I = 50 μA, 60 μA, 80 μA, 100 μA, 200 μA, 400 μA, 1 mA and 2 mA); for pulse width 0.5 ms the stimulation current ranged from 0.1 mA up to 2 mA (I = 0.1, 0.2, 0.5, 1 and 2 mA). For high-frequency analysis of the evoked activity on the sciatic nerve, the raw data corresponding to the two channels of interest (one for each microwire) for each stimulation protocol was first band-pass filtered between 200 and 7000 Hz (9th order, zero phase butterworth filter), to match the bandwidth of CAPs and to reduce out-of-band noise. Stimulation artefacts were detected from each electrode by setting a threshold of 4.5 times the standard deviation. A window of 2 ms before and 50 ms after the maximum of each artefact was extracted, and the corresponding waveforms were averaged across time to get an averaged profile of the CAPs comprising the elicited response obtained with each microwire. The CAP waveform analysis for each profile shows distinct fibre velocity bands, which were studied to see how they are affected by different stimulation protocols, and how the resolution of the peaks in each band was affected by the presence or absence of PEDOT coating. In addition, a region of 2 seconds prior to the first stimulation pulse was selected as baseline. The standard deviation of this region was calculated for each wire and stimulation protocol and was used as an estimate of the background noise. The differences in this metric were compared between pairs of microwires to evaluate their performance.

For brain recordings, the brain screw was used as the reference electrode. The large surface of the exposed tips limited the acquisition of single units from the barrel cortex. Therefore, local field potentials were analysed. The recordings were first downsampled to 10 kHz, and low-pass filtered with a cut-off frequency of 200 Hz (9th order, zero phase butterworth filter), which is the maximum frequency expected from the low-frequency components of the extracellular field potential. A notch filter was used to remove any line interference at 50 Hz and its odd harmonic at 150 Hz. For each device (*i.e.* pair of microwires with different coatings) a clear profile of periods of rest followed by periods of neural activity was observed. Each rest and activity pair was defined as a window of a minimum of two seconds of baseline followed by another >2 seconds window, and each pair was considered an observation. For each wire, the signal-to-noise ratio (SNR) for each observation was calculated using the ratio of the variance of the signal during the period of activity by the variance of the signal during the period of rest, which was assumed to be baseline noise.

$$\mathrm{SNR\ (dB)} = 10 \times \log(\mathrm{var(sig)}/\mathrm{var(noise)})$$

The maximum value of the signal during the activity windows was also extracted for each microwire. These two metrics, SNR and the variance of the signal on the activity periods (VAR), extracted from the multiple observations (more than 20 per device) were compared between the two microwires.

Statistical analysis. In both *in vivo* electrophysiology experiments, recording from the sciatic nerve and the barrel cortex, two microwires with different PEDOT coatings were simultaneously compared. For the sciatic nerve recordings, the standard deviation of the baseline noise was extracted for each pair of microwires at each stimulation protocol, which was considered independent observations. For the brain recordings, the SNR and the maximum value of the activity signal were extracted from each rest-activity pair (*i.e.* observation) for the two microwires. In both cases, we are interested in comparing the mean values of each metric for all the observations made by each pair of microwires. Therefore, paired statistical tests were selected to compare the significance of the differences between the extracted metrics for each microwire. To begin with, the Shapiro–Wilk test was applied to each group (collection of observations for each metric and microwires) to evaluate the criteria of normality (*i.e.* whether the data comes from a normal distribution). Then, the Levene's test was used to check for equal variances. If these two conditions were met, the parametric paired t-test was applied to determine pairwise differences. Otherwise, the non-parametric wilcoxon signed-rank test was used. The significance level was set at $p < 0.05$. The statistical analysis was performed using the python library statsmodels.

5. Conclusion

Conductive-polymer implantable microelectrode systems are a growing field of neuroscience research.[69–71] However, their fabrication requires highly specialised equipment and know-how, and the few commercialised options are costly, limiting their accessibility for some researchers. In this work we have demonstrated for the first time a simple and inexpensive strategy to coat W-microwires with PEDOT conducting polymer, making it an effective and accessible tool in electrophysiology studies. We have found that the preconditioning of W-microwires through annealing to generate oxidized species is necessary for the successful electropolymerization of PEDOT by facilitating its nucleation. The morphology of the W/PEDOT microwires was more homogeneous than that of the Au/PEDOT microwires for the same coating procedure. We have also found that PEDOT decreases the impedance values and increments the capacitance one or two orders order of magnitude if compared with bare metals. The improved properties of the

Open Access Article. Published on 04 detsember 2023. Downloaded on 01.02.2026 10:58:51.
This article is licensed under a Creative Commons Attribution 3.0 Unported Licence.

W/PEDOT microwires were also explored in pre-clinical studies to enhance the accuracy and reliability of acute electrophysiology recordings of local field potentials in the brain and compound action potentials in the sciatic nerve. Further research is required to assess the biocompatibility and potential benefits and limitations of these devices in chronic experimental setups.

Author contributions

Conceptualization, investigation, data curation, visualization, writing the original draft and editing the manuscript: A. Güemes and A. Dominguez-Alfaro; formal analysis and software: A. Güemes; investigation: R. Mizuta, S. Velasco-Bosom; validation: A. Carnicer-Lombarte; supervision: G. Malliaras and D. Mecerreyes; fundings acquisition and resources: G. Malliaras; methodology: D. G. Barone. All authors have contributed to reviewing the manuscript.

Data availability statements

The code for the analysis of neurograms can be found at A. Güemes, 2023, GitHub, with DOI **https://doi.org/10.5281/zenodo.8000178**.

Conflicts of interest

There are no conflicts to declare.

Acknowledgements

A. Güemes acknowledges funding support from the Royal Commission for the Exhibition of 1851. A. Dominguez-Alfaro acknowledges UPV/EHU for funding transferred by the European Union-Next Generation EU by the Margarita Salas fellowship. (MARSA N° agreement 22/77). A. Carnicer-Lombarte acknowledges support from the University of Cambridge for a Borysiewicz Interdisciplinary Fellowship. S. Velasco-Bosom and G. Malliaras acknowledge support by the NIHR Cambridge Biomedical Research Centre (NIHR203312). The views expressed are those of the author(s) and not necessarily those of the NIHR or the Department of Health and Social Care. This work was supported by Marie Sklodowska-Curie Research and Innovation Staff Exchanges (RISE) under grant agreement no. 823989 ''IONBIKE''. For the purpose of open access, the authors have applied a Creative Commons Attribution (CC BY) licence to any Author Accepted Manuscript version arising from this submission.

References

1 A. Jackson and E. E. Fetz, *J. Neurophysiol.*, 2007, **98**, 3109–3118.
2 M. P. Ward, P. Rajdev, C. Ellison and P. P. Irazoqui, *Brain Res.*, 2009, **1282**, 183–200.
3 L. D. Kolibius, F. Roux, G. Parish, M. Ter Wal, M. Van Der Plas, R. Chelvarajah, V. Sawlani, D. T. Rollings, J. Lang, S. Gollwitzer, K. Walther, R. Hopfengärtner, G. Kreiselmeyer, H. Hamer, B. P. Staresina, M. Wimber, H. Bowman and S. Hanslmayr, *bioRxiv*, DOI: **10.1101/2021.06.28.450149**.
4 S. Elyahoodayan, W. Jiang, C. D. Lee, X. Shao, G. Weiland, J. J. Whalen, A. Petrossians and D. Song, *Front. Neurosci.*, 2021, **15**, 616063.
5 Z. J. Du, C. L. Kolarcik, T. D. Y. Kozai, S. D. Luebben, S. A. Sapp, X. S. Zheng, J. A. Nabity and X. T. Cui, *Acta Biomater.*, 2017, **53**, 46–58.
6 G. Lehew and M. A. L. Nicolelis, *Methods Neural Ensemble Recordings*, 2008, **2**, 361–371.
7 J. D. Falcone, T. Liu, L. Goldman, L. Rieth, C. E. Bouton, M. Straka and H. S. Sohal, *J. Neural Eng.*, 2020, **17**, 46003.
8 J. D. Falcone, T. Liu, L. Goldman, D. D. Pogue, M. Straka, L. Rieth, C. E. Bouton and H. S. Sohal, bioRxiv, 2018, 402925.
9 B. Kim, A. Reyes, B. Garza and Y. Choi, *Microsyst. Technol.*, 2015, **21**, 1551–1557.
10 J. C. Williams, J. A. Hippensteel, J. Dilgen, W. Shain and D. R. Kipke, *J. Neural Eng.*, 2007, **4**, 410.
11 E. Patrick, M. E. Orazem, J. C. Sanchez and T. Nishida, *J. Neurosci. Methods*, 2011, **198**, 158–171.
12 J. C. Sanchez, N. Alba, T. Nishida, C. Batich and P. R. Carney, *IEEE Trans. Neural Syst. Rehabil. Eng.*, 2006, **14**, 217–221.
13 A. Shah Idil and N. Donaldson, *J. Neural Eng.*, 2018, **15**, 21006.
14 D. Mantione, I. del Agua, A. Sanchez-Sanchez and D. Mecerreyes, *Polymers*, 2017, **9**, 354.
15 C. M. Proctor, J. Rivnay and G. G. Malliaras, *J. Polym. Sci., Part B: Polym. Phys.*, 2016, **54**, 1433–1436.
16 J. Rivnay, S. Inal, B. A. Collins, M. Sessolo, E. Stavrinidou, X. Strakosas, C. Tassone, D. M. Delongchamp and G. G. Malliaras, *Nat. Commun.*, 2016, **7**, 11287.
17 D. Khodagholy, T. Doublet, P. Quilichini, M. Gurfinkel, P. Leleux, A. Ghestem, E. Ismailova, T. Hervé, S. Sanaur, C. Bernard and G. G. Malliaras, *Nat. Commun.*, 2013, **4**, 1575.
18 A. Madhan Kumar, M. A. Hussein, A. Y. Adesina, S. Ramakrishna and N. Al-Aqeeli, *RSC Adv.*, 2018, **8**, 19181–19195.
19 A. M. Kumar, A. Khan, M. A. Hussein, M. Y. Khan, H. Dafalla, B. Suresh and S. Ramakrishna, *Prog. Org. Coat.*, 2022, **170**, 106946.
20 S. Venkatachalam, M. Depriester, A. H. Sahraoui, B. Capoen, M. R. Ammar and D. Hourlier, *Carbon N Y*, 2017, **114**, 134–140.
21 C.-Y. Su and H.-C. Lin, *J. Phys. Chem. C*, 2009, **113**, 4042–4046.
22 Z. S. Houweling, J. W. Geus and R. E. I. Schropp, *Mater. Chem. Phys.*, 2013, **140**, 89–96.
23 E. Besozzi, D. Dellasega, V. Russo, C. Conti, M. Passoni and M. G. Beghi, *Mater. Des.*, 2019, **165**, 107565.
24 A. Dominguez-Alfaro, I. Jénnifer Gómez, N. Alegret, D. Mecerreyes and M. Prato, *Polymers*, 2021, **13**(3), 436.

© 2023 The Author(s). Published by the Royal Society of Chemistry

Open Access Article. Published on 04 detsember 2023. Downloaded on 01.02.2026 10:58:51.
This article is licensed under a Creative Commons Attribution 3.0 Unported Licence.

25 J. Heinze, B. A. Frontana-Uribe and S. Ludwigs, *Chem. Rev.*, 2010, **110**, 4724–4771.
26 D. J. Fermín and B. R. Scharifker, *J. Electroanal. Chem.*, 1993, **357**, 273–287.
27 J. Heinze, A. Rasche, M. Pagels and B. Geschke, *J. Phys. Chem. B*, 2007, **111**, 989–997.
28 G. Zotti, S. Zecchin, G. Schiavon and A. Berlin, *Chem. Mater.*, 2002, **14**, 3607–3614.
29 J. Hagler, J. Yeu, X. Zhou, G. Ducharme, B. Amilhon and F. Cicoira, *Adv. Mater. Interfaces*, 2022, **9**, 2201066.
30 N. Rossetti, P. Luthra, J. Hagler, A. H. Jae Lee, C. Bodart, X. Li, G. Ducharme, F. Soavi, B. Amilhon and F. Cicoira, *ACS Appl. Bio Mater.*, 2019, **2**, 5154–5163.
31 C. Bodart, N. Rossetti, J. Hagler, P. Chevreau, D. Chhin, F. Soavi, S. B. Schougaard, F. Amzica and F. Cicoira, *ACS Appl. Mater. Interfaces*, 2019, **11**, 17226–17233.
32 N. Elgrishi, K. J. Rountree, B. D. McCarthy, E. S. Rountree, T. T. Eisenhart and J. L. Dempsey, *J. Chem. Educ.*, 2018, **95**, 197–206.
33 K. Wijeratne, U. Ail, R. Brooke, M. Vagin, X. Liu, M. Fahlman and X. Crispin, *Proc. Natl. Acad. Sci. U. S. A.*, 2018, **115**, 11899–11904.
34 V. S. Vasantha and S. M. Chen, *Electrochim. Acta*, 2005, **51**, 347–355.
35 E. Er, H. Çelikkan and N. Erk, *Sens. Actuators, B*, 2017, **238**, 779–787.
36 M. Bianchi, A. De Salvo, M. Asplund, S. Carli, M. Di Lauro, A. Schulze-Bonhage, T. Stieglitz, L. Fadiga and F. Biscarini, *Adv. Sci.*, 2022, **9**, 2104701.
37 G. Dijk, A. L. Rutz and G. G. Malliaras, *Adv. Mater. Technol.*, 2020, **5**, 1900662.
38 N. A. Alba, Z. J. Du, K. A. Catt, T. D. Y. Kozai and X. T. Cui, *Biosensors*, 2015, **5**, 618–646.
39 T. D. Y. Kozai, K. Catt, Z. Du, K. Na, O. Srivannavit, M. H. Razi-ul, J. Seymour, K. D. Wise, E. Yoon and X. T. Cui, *IEEE Trans. Biomed. Eng.*, 2015, **63**, 111–119.
40 N. Rossetti, J. Hagler, P. Kateb and F. Cicoira, *J. Mater. Chem. C*, 2021, **9**, 7243–7263.
41 J. E. Hagler, J. Yeu, X. Zhou, G. Ducharme, B. Amilhon and F. Cicoira, *Adv. Mater. Interfaces*, 2022, **9**(35), 2201066.
42 N. Rossetti, P. Luthra, J. Hagler, A. H. Jae Lee, C. Bodart, X. Li, G. Ducharme, F. Soavi, B. Amilhon and F. Cicoira, *ACS Appl. Bio Mater.*, 2019, **2**, 5154–5163.
43 J. E. Collazos-Castro, G. R. Hernández-Labrado, J. L. Polo and C. García-Rama, *Biomaterials*, 2013, **34**, 3603–3617.
44 H. Vara and J. E. Collazos-Castro, *Acta Biomater.*, 2019, **90**, 71–86.
45 F. Tian, J. Yu, W. Wang, D. Zhao, J. Cao, Q. Zhao, F. Wang, H. Yang, Z. Wu, J. Xu and B. Lu, *J. Colloid Interface Sci.*, 2023, **638**, 339–348.
46 T. Xu, W. Ji, X. Wang, Y. Zhang, H. Zeng, L. Mao and M. Zhang, *Angew. Chem., Int. Ed.*, 2022, **61**, e202115074.
47 T. Xu, W. Ji, Y. Zhang, X. Wang, N. Gao, L. Mao and M. Zhang, *Angew. Chem., Int. Ed.*, 2022, **61**, e202204344.
48 M. Patros, M. M. Ottaviani, L. Wright, T. Dawood and V. G. Macefield, *J. Physiol.*, 2022, **600**, 3113–3126.
49 M. Berggren and G. G. Malliaras, *Science*, 2019, **364**, 233–234.
50 M. Han, S. B. Srivastava, E. Yildiz, R. Melikov, S. Surme, I. B. Dogru-Yuksel, I. H. Kavakli, A. Sahin and S. Nizamoglu, *ACS Appl. Mater. Interfaces*, 2020, **12**, 42997–43008.
51 A. R. Harris, *J. Neural Eng.*, 2021, **18**(2), 025001.
52 J. E. Ferguson, C. Boldt and A. D. Redish, *Sens. Actuators, A*, 2009, **156**, 388–393.
53 E. S. Kappenman and S. J. Luck, *Psychophysiology*, 2010, **47**, 888–904.
54 K. A. Ludwig, J. D. Uram, J. Yang, D. C. Martin and D. R. Kipke, *J. Neural Eng.*, 2006, **3**, 59–70.
55 K. A. Ludwig, N. B. Langhals, M. D. Joseph, S. M. Richardson-Burns, J. L. Hendricks and D. R. Kipke, *J. Neural Eng.*, 2011, **8**(1), 014001.
56 J. P. Neto, P. Baião, G. Lopes, J. Frazão, J. Nogueira, E. Fortunato, P. Barquinha and A. R. Kampff, *Front. Neurosci.*, 2018, **12**, DOI: **10.3389/fnins.2018.00715**.
57 S. Suner, M. R. Fellows, C. Vargas-Irwin, G. K. Nakata and J. P. Donoghue, *IEEE Trans. Neural Syst. Rehabil. Eng.*, 2005, **13**, 524–541.
58 A. Merz and M. Rohwerder, *J. Electrochem. Soc.*, 2019, **166**, C314–C320.
59 A. Merz, M. Uebel and M. Rohwerder, *J. Electrochem. Soc.*, 2019, **166**, C304–C313.
60 E. M. Thaning, M. L. M. Asplund, T. A. Nyberg, O. W. Inganäs and H. Von Holst, *J. Biomed. Mater. Res., Part B*, 2010, **93**, 407–415.
61 F. Tian, J. Yu, W. Wang, D. Zhao, J. Cao, Q. Zhao, F. Wang, H. Yang, Z. Wu, J. Xu and B. Lu, *J. Colloid Interface Sci.*, 2023, **638**, 339–348.
62 C. Boehler, D. M. Vieira, U. Egert and M. Asplund, *ACS Appl. Mater. Interfaces*, 2020, **12**, 14855–14865.
63 E. Jan, J. L. Hendricks, V. Husaini, S. M. Richardson-Burns, A. Sereno, D. C. Martin and N. A. Kotov, *Nano Lett.*, 2009, **9**, 4012–4018.
64 X. T. Cui and D. D. Zhou, *IEEE Trans. Neural Syst. Rehabil. Eng.*, 2007, **15**, 502–508.
65 V. Jadkar, A. Pawbake, R. Waykar, A. Jadhavar, A. Date, D. Late, H. Pathan, S. Gosavi and S. Jadkar, *Phys. Status Solidi A*, 2017, **214**, 1600717.
66 A. J. Bard, L. R. Faulkner and H. S. White, *Electrochemical methods: fundamentals and applications*, John Wiley & Sons, 2022.
67 R. S. Nicholson, *Anal. Chem.*, 1965, **37**, 1351–1355.
68 S. Middya, A. Carnicer-Lombarte, V. F. Curto, S. Hilton, A. Genewsky, A. L. Rutz, D. G. Barone, G. S. Kaminski Schierle, A. Sirota and G. G. Malliaras, *Adv. Electron. Mater.*, 2022, 2200883.
69 L. Merken, M. Schelles, F. Ceyssens, M. Kraft and P. Janssen, *J. Neural Eng.*, 2022, **19**, 66039.
70 S. Middya, V. F. Curto, A. Fernández-Villegas, M. Robbins, J. Gurke, E. J. M. Moonen, G. S. Kaminski Schierle and G. G. Malliaras, *Adv. Sci.*, 2021, **8**, 2004434.
71 W. Lee, D. Kim, N. Matsuhisa, M. Nagase, M. Sekino, G. G. Malliaras, T. Yokota and T. Someya, *Proc. Natl. Acad. Sci. U. S. A.*, 2017, **114**, 10554–10559.

© 2023 The Author(s). Published by the Royal Society of Chemistry